03

Turbulence mixing computational and experimental modeling of coolant flows with different temperatures

© N.V. Matsin,[1] R.R. Ryazapov,[2] A.E. Sobornov,[1] A.V. Kotin[1]

[1] Alekseev State Technical University,
603155 Nizhny Novgorod, Russia
[2] Federal Research Center A.V. Gaponov-Grekhov Institute of Applied Physics of the Russian Academy of Sciences,
603950 Nizhny Novgorod, Russia
e-mail: lebron.09@mail.ru

Received September 2, 2025
Revised October 6, 2025
Accepted November 1, 2025

The experimental model reproduces configuration flow part to the high-temperature one with a coefficient of geometric similarity $K = 4/3$. The „dye injection“method was used to visualize the flow in the mixing region. The LES approach for the spatial and temporal resolution of turbulent structures was used. Unresolved scales description in Ansys Fluent was carried out by the WALE subgrid-scale model, in FlowVision software the Smagorinsky model was applied. It was shown that the WALE model mathematical formulation combined with block-structured mesh ensures better adaptation to variations in task input parameters. Temperature fluctuations power spectral density distributions in the inertial interval follow the „$-5/3$“law characteristic of a passive scalar in locally isotropic turbulence. Turbulent kinetic energy distributions evaluation has uncovered vortex structures mechanism during mixing process. Analysis showed that FlowVision software is less accurate in simulating crucial features of the mixing process. The obtained data will be used for further mixing process calculating at the pressurized water reactor (PWR) operating parameters.

Keywords: temperature fluctuations, scale-resolving simulation, turbulent kinetic energy, Y-junction, spectral analysis

DOI: 10.61011/TP.2026.04.63259.253-25

Introduction

A tendency to an increase of unit power of reactor plants imposes higher requirements to lifetime reliability of NPP equipment. High heat intensity of modern heat-exchange equipment causes presence of nonstationary temperature gradients in a heat-conducting surface wall and, therefore, temperature stresses. At the temperatures that are typical for nuclear power plants (NPP), yield strength of materials is greatly reduced [1], while presence of high-intensity fluctuations of a temperature field results in origination of irreversible local deformations of the heat-exchange surface, thereby increasing a damage accumulation rate and reducing equipment lifetime.

Experience in operation of main NPP equipment has demonstrated that processes of mixing of coolant flows with different temperatures are especially important and that they affect fatigue durability of structural materials [2]. A random transfer of momentum within a mixing area predetermines presence of temperature fluctuations near the wall, which often crucially affect on structural elements lifetime. Most experimental studies of the mixing process were principally on models with a T-shaped configuration of a flow part within a narrow range of regime parameters [3–5], thereby making it difficult to determine specifics of a process of heat-force loading under NPP operating conditions. In this case, it is promising to apply numerical methods, which make it possible to resolve spatiotemporal specific features of the coolant temperature field and a stress-strain state of the material in detail, which will finally make it possible to determine equipment elements lifetime. Based on existing mathematical models, it is possible to create a universal computational technique for estimating lifetime characteristics. But complexity of the simulated process necessitates validation of the technique at various stages.

Using a high-temperature bench, a science team of the laboratory „Steam-generating systems“ of Nizhny Novgorod State Technical University n.a. R.E. Alekseev experimentally studies the mixing process in a Y-junction with counter motion of single-phase coolant flows and, in the same conditions, lifetime tests at NPP standard parameters [6,7]. The studies are characterized by an original design of the experimental branch, which provides localization of a zone with the highest value of a mean-square amplitude of the temperature fluctuations. It is untruly to validate a CFD-model based only on experimental data about the coolant temperature field in the mixing zone. Along with analysis of the temperature field, in order to substantiate representativity of the calculation results, it is also necessary to study mixing process hydrodynamics specific features and their influence on development of thermal fluctuations. For this purpose, the science team has simulated a flow structure on a training-study bench, whose experimental model is geometrically similar to the experimental branch of

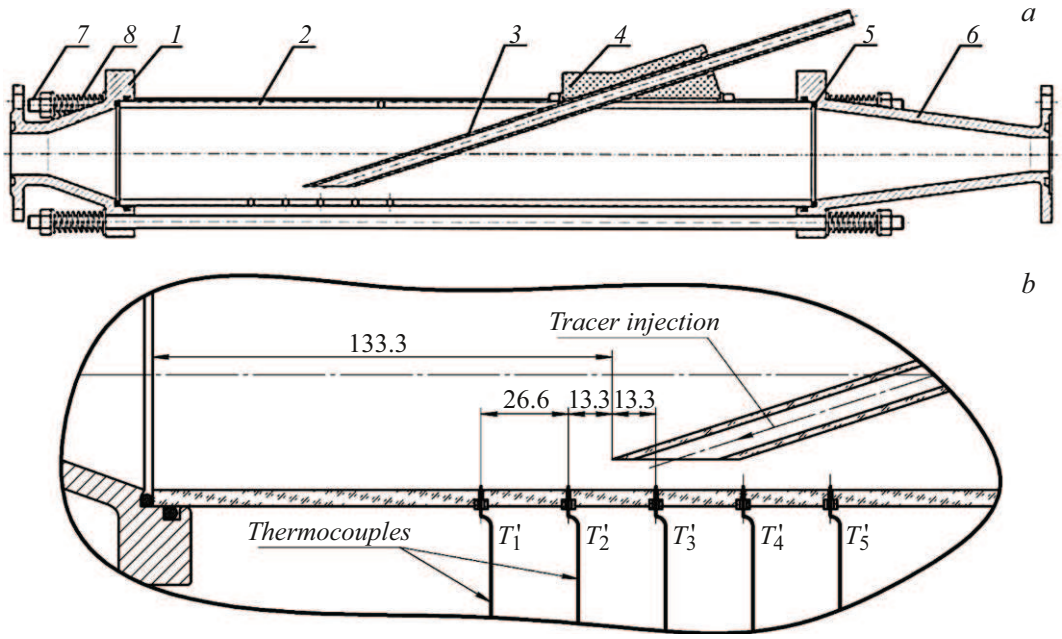

Figure 1. General view of the experimental model (a) and an arrangement of the thermocouples (b): *1* — the guiding flange, *2* — the main pipe, *3* — the peripheral pipe, *4* — the bandage, *5* — the gasket, *6* — the outlet flange, *7* — the stud, *8* — the spring.

the high-temperature bench [8,9]. Dynamics of large-scale eddy structures in the area of thermocouples was studied using a „dye injection" method. A tracer was a hydrophilic ink solution. To continue a study described in [8], a series of refining experiments was done on an updated experimental unit. The present study has numerically simulated the mixing process using Ansys Fluent software. Besides, under implementation of the import substitution program aimed at developing Russian designs in the field of computational hydrodynamics, it was also simulated using FlowVision software. The velocity and temperature fields fluctuations spectrum was resolved by applying a Large Eddy Simulation method (LES). High-frequency disturbances were simulated in Ansys Fluent using a subgrid wall-adapting local eddy viscosity model (WALE), whose mathematical formulation quite precisely reproduces specific features of turbulent heat transfer in a limited space [10–12]. The FlowVision software is based on the Smagorinsky model (Sm) [13] for simulating small-scale turbulence. The series of the calculations was done to validate the computational model based on results of a simulation experiment.

1. Experimental study

The thermal and hydrodynamic characteristics of mixing the coolant flows was experimentally simulated on the additional bench. The bench was described in detail in [9]. A modern bench updating stage consisted of the following:

— replacement of a tubular electrical heater with a more productive analogue of power of 3 kW, thereby making it possible to provide a high rate of heating speed and to maintain the required cooling temperature within the wide range of the regime parameters;

— replacement of a LZM-8T rotameter with a pulse flowrate meter YF-S401 having a measurement range 0.3−6 l/min. It made it possible to automatically data record implementations of a „cold" flowrate in synchrony with other parameters, thereby simplifying a data processing.;

— to design and installation an improved design of a dispenser, which is advantageous in a uniform injection of the contrast tracer during more than 100 s

The model for experimental simulation is replica of a high-temperature original design model (Fig. 1, a) can be used for the mixing process specific features simulation [7]. Structurally, the Y-junction assembly consists of the main 80×5 mm and peripheral 12×2 mm plexiglass pipes, the guiding and outlet flanges, fasteners and other elements. The peripheral tube is oriented at the angle of 18° to an axis of the main pipe. The distance from a peripheral tube cut to the internal wall of the main one is (9.3 ± 0.5) mm. The guiding flange includes a diffusor with an opening angle of 40°, which is designed for forming a separation stream of the „hot" flow in the mixing area. The distance from an outlet edge of the diffusor to a front edge of the peripheral pipe is (133.3 ± 0.5) mm. The channel shape of the experimental model is geometrically similar to the experimental branch of the NNSTU high-temperature bench. A coefficient of geometrical similarity is $K = 4/3$ [9].

Dynamics of the eddy structures in the mixing area was studied by a visual method by injecting the contrast tracer into the flow. A tracing fluid, which is an aqueous solution of stationary ink with 50 % concentration, was continuously injected into the mixing area through the peripheral tube by

means of the dispenser. A relative fraction of the tracer did not exceed 0.4 % of the flowrate value of the „cold“ flow of the coolant. Along with tracer injection, the studied process was video-recorded at the rate of 100 frames per second.

In synchrony with visualization of the mixing process, the coolant temperature field was measured. Temperature sensors were fast-response chromel-alumel (type K) thermocouples made of a steel cable with mineral insulation with a sensitive part's diameter of 0.5 mm. The sensors provide measurement of the temperature with an error $\pm 0.5\,^{\circ}$C.The implementation length was ≈ 150 s at the average frequency of thermocouples' request $f = 8$ Hz. The arrangement of the thermocouples is shown in Fig. 1, *b*.

Application of plexiglass included in the experimental model imposes a limitation to an allowable temperature of the coolant, whose upper limit is accepted to be 75,°C.

The ranges of the regime parameters of experimental simulation included:

— Reynolds number for the „hot“ flow at the inlet $\mathrm{Re}_h = (6.8-7.1)\cdot 10^4$, downstream of the diffusor $\mathrm{Re}_h = (3-3.2)\cdot 10^4$;

— Reynolds number for the „cold“ flow $\mathrm{Re}_c = 790-3050$;

— the temperature of the „hot“ flow $T_h = 72 \pm 2\,^{\circ}$C;

— the temperature of the „cold“ flow $T_c = 22-52\,^{\circ}$C;

— coolant pressure $P_{abc} = 1.125$ atm.

2. Numerical simulation

A general view of the geometrical model with indicating boundary conditions is shown in Fig. 2.

Due to a low thermal conductivity coefficient of organic glass $\lambda = 0.2-0.3$ W/(m·K) the team of the authors decided to omit the process of heat transfer between the „hot“ and „cold“ flows, thereby making it possible to neglect a finite-element part of the model, which corresponded to the peripheral tube.

Turbulence was simulated using the LES-approach. Under the LES, the large-scale turbulent structures are precisely resolved, while description of the small-scale structure and their interaction with the large ones is simulated. Spatiotemporal anisotropy of the large eddy structures substantially contributes to development of a fluctuation process, therefore it is critically important to precisely resolve them when analyzing thermal and hydrodynamic

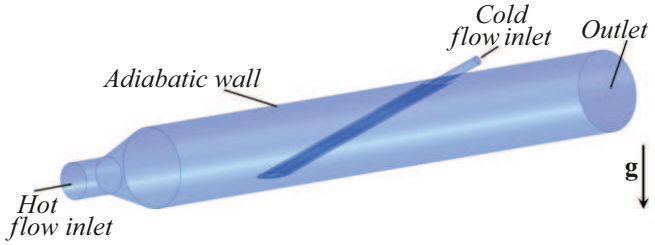

Figure 2. General view of the geometrical model.

parameters. The eddies are divided into the large and small ones at the stage of filtration of the Navier-Stokes equations. In implicit filtration, a scale limiter is a mesh size of the grid model. The eddy structures, whose size is smaller than the mesh size, are not resolved, but they are simulated by means of a subgrid stress tensor [14]:

$$\tau_{ij} = \rho\overline{U_i U_j} - \rho\overline{U_i}\,\overline{U_j}, \tag{1}$$

where ρ is a density of the medium; $\overline{U_i U_j}$ is a filtered product of components of an instantaneous velocity; $\overline{U_i}$, $\overline{U_j}$ are values of the components of the filtered velocity.

The equation for LES are obtained by filtering the Navier-Stokes equation in space and consist of equation of momentum (2), continuity (3) and transfer of thermal energy (4), (5) [15]:

$$\frac{\partial}{\partial t}(\rho\overline{U_i}) + \frac{\partial}{\partial x_j}(\rho\overline{U_i}\,\overline{U_j}) = -\frac{\partial\overline{P}}{\partial x_i} + \mu\frac{\partial}{\partial x_j}\left(\left[\frac{\partial\overline{U_i}}{\partial x_j} + \frac{\partial\overline{U_j}}{\partial x_i}\right] - \frac{2}{3}\frac{\partial\overline{U_l}}{\partial x_l}\delta_{ij}\right) - \frac{\partial\tau_{ij}}{\partial x_j} + (\rho - \rho_r)g_i, \tag{2}$$

$$\frac{\partial\rho}{\partial t} + \frac{\partial}{\partial x_i}(\rho\overline{U_i}) = 0, \tag{3}$$

$$\frac{\partial}{\partial t}(\rho\overline{h}) + \frac{\partial}{\partial x_j}(\rho\overline{U_j}\,\overline{h}) = \frac{\partial}{\partial x_j}\left(\left(\lambda + \frac{\mu_t}{\mathrm{Pr}_t}C_P\right)\frac{\partial\overline{T}}{\partial x_j}\right), \tag{4}$$

$$\overline{h} = \int_{298.15}^{\overline{T}} C_P dT, \tag{5}$$

where indices $i = 1, 2, 3$ and $j = 1, 2, 3$ — indicate directions of the Cartesian system of coordinates x_i; μ, λ, C_p — dynamic viscosity, thermal conductivity and heat capacity of the medium are functions of the temperature; t is time; δ_{ij} is a unit tensor; $\rho_r = 976.6$ kg/m^3 is the density of the liquid in a reference point; $g\,(0; -9.81; 0)$ m/s^2 is a vector of gravitational acceleration; μ_t is subgrid turbulent viscosity; $\mathrm{Pr}_t = 0.85$ is a turbulent Prandtl number; $\overline{h}$ is filtered static enthalpy; $\overline{T}$ is the filtered temperature; $\overline{P}$ is filtered pressure.

In order to close a system of determinant equations and take into account a high-frequency part of the turbulence spectrum, the Subgrid–Scale (SGS) models are used, wherein most of them are based on a generalized Boussinesq hypothesis (6) [16], which assumes a linear relation between the subgrid stress tensor τ_{ij} and a tensor of the filtered field strain rates $\overline{S}_{ij}$ (7):

$$\tau_{ij} = \frac{1}{3}\tau_{kk}\delta_{ij} - 2\mu_t\overline{S}_{ij}, \tag{6}$$

$$\overline{S}_{ij} = \frac{1}{2}\left(\frac{\partial\overline{U_i}}{\partial x_j} + \frac{\partial\overline{U_j}}{\partial x_i}\right), \tag{7}$$

where τ_{kk} is an isotropic part of the subgrid stresses.

The WALE subgrid model based on a square of the velocity gradient tensor uses the following relationship for calculating μ_t:

$$\mu_t = \rho L_s^2 \frac{(S_{ij}^d S_{ij}^d)^{3/2}}{(\overline{S}_{ij}\overline{S}_{ij})^{5/2} + (S_{ij}^d S_{ij}^d)^{5/4}}, \quad (8)$$

$$L_s = \min(kd, C_\omega h), \quad (9)$$

$$h = (\Delta x \cdot \Delta y \cdot \Delta z)^{1/3}, \quad (10)$$

where L_s is a mixing length calculated as a minimum of two complexes: a product of the Karman constant $k - 0.41$ and a distance to the nearest wall d, a product of the WALE model constant $C_\omega = 0.325$ and a linear mesh size h; $\Delta x, \Delta y, \Delta z$ are mesh sizes along the axes of the Cartesian system of coordinates; S_{ij}^d is a traceless symmetric part of the square of the velocity gradient tensor, which is calculated according to (11) [17]:

$$S_{ij}^d = \frac{1}{2}\left(\frac{\partial \overline{U}_i}{\partial x_k}\frac{\partial \overline{U}_k}{\partial x_j} + \frac{\partial \overline{U}_j}{\partial x_k}\frac{\partial \overline{U}_k}{\partial x_i}\right) - \frac{1}{3}\delta_{ij}\frac{\partial \overline{U}_l}{\partial x_k}\frac{\partial \overline{U}_k}{\partial x_l},$$

$$\frac{\partial \overline{U}_i}{\partial x_k}\frac{\partial \overline{U}_k}{\partial x_j} = g_{ij}^{-2}, \quad (11)$$

where g_{ij}^{-2} is the square of the velocity gradient tensor.

An antisymmetric part of the velocity gradient tensor is a vorticity tensor $\overline{\Omega}_{ij}$

$$\overline{\Omega}_{ij} = \frac{1}{2}\left(\frac{\partial U_i}{\partial x_j} - \frac{\partial U_j}{\partial x_i}\right). \quad (12)$$

The tensor determined by the relationship (11) can be rewritten through $\overline{S}$ and $\overline{\Omega}$ as follows:

$$S_{ij}^d = \overline{S}_{ik}\overline{S}_{kj} + \overline{\Omega}_{ik}\overline{\Omega}_{kj} - \frac{1}{3}\delta_{ij}[S_{mn}S_{mn} - \Omega_{mn}\Omega_{mn}]. \quad (13)$$

The expression (13) takes into account both a local strain rate as well as a rotational speed. Consequently, a spatial operator (8) detect all turbulent structures related to dissipation of kinetic energy [14]. The complex $(\overline{S}_{ij}\overline{S}_{ij})^{5/2}$ prevails in an area of a viscous sublayer, where a shear rate is high, whereas $(S_{ij}^d S_{ij}^d)^{3/2}$ becomes higher than $(\overline{S}_{ij}\overline{S}_{ij})^{5/2}$ in a logarithmic area of the boundary layer. Thus, eddy viscosity naturally tends to zero near the wall, which does not require introduction of a special damper function, and significantly increases in the turbulent boundary layer. Tensor invariance of the magnitude $S_{ij}^d S_{ij}^d$ makes it possible to adapt the WALE model to transformation of the system of coordinates, using only local information (without defining the nearest point in the grid). As a result, a set of the said specific features of the model makes it possible to quite precisely reproduce the fluctuation process in the area downstream of the diffusor and in the mixing zone.

For describing unresolved scales, the FlowVison software implements, under the LES approach, a Sm model based on the second invariant of the symmetric part $\overline{S}_{ij}$ of the velocity gradient tensor. In this case, subgrid turbulent viscosity μ_t is calculated according to (14) [13]:

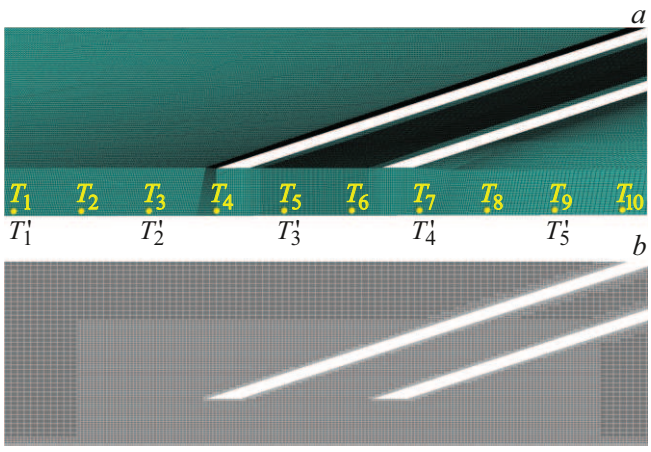

Figure 3. Grid model in the flow mixing area, which is constructed in Ansys ICEM CFD (a) and the automatic grid generator of FlowVision (b). $T_1 - T_{10}$ — monitoring points of the computational models; $T_1 - T_5$ locations of the thermocouples in the experimental model.

$$\mu_t = \rho(C_s h)^2 |\overline{S}|, \quad (14)$$

where $C_s = 0.1$ is a Smagorinsky constant [17]; $|\overline{S}| = \sqrt{2\overline{S}_{ij}\overline{S}_{ij}}$ is a modulus of the strain rate tensor.

It has been numerically simulated in Ansys Fluent based on a finite-volume grid model (Fig. 3, a) constructed by a unit topology principle in the Ansys ICEM CFD software. Created elements of a „quasicubic“ form made it possible to orient a grid model along a direction of the flows and, as a result, to reduce influence of numerical diffusion on accuracy of a solution of the differential equations. According to an architecture of an Ansys Fluent solver, the initial structured grid was converted into an unstructured format, while keeping key advantages of the structured approach at the same time. No thickening of the grid model near the wall is related to slight influence (due to remoteness) of a near-wall area on development of the fluctuation process. A value of a dimensionless distance to the wall in the flow mixing area was $y^+ \approx 8$ and in this case Ansys Fluent activates a unified wall law as per B.A. Kader [15]. A model discretization degree is 34.5 million cells. The Reynolds number calculated by a wall friction velocity was $\mathrm{Re}_{\tau\_\mathrm{mix}} \approx 240$ in a flow collision area. Due to formation of the boundary layer, along a direction of motion of the „hot“ flow, there is an observed growth of time-averaged wall friction stress and an observed natural increase of $\mathrm{Re}_{\tau\_\mathrm{out}} \approx 1200$ in the points T_9 and T_{10}.

An automatic grid generator of the FlowVision software builds predominantly hexagonal cells by approximating curved boundaries by means of subgrid geometry resolution [18]. The model was initially discretized by dividing into elements along the axes of the Cartesian system of

coordinates: the axes „X“ and „Y“ — 100 elements; the axis „Z“ — 1000 elements. For quality resolution of the fluctuation process in the diffusor area and the mixing zone (Fig. 3, *b*), the grid model was adapted at the first level. Around the walls, it was adapted at the second level. Dimension of the grid model is 17.5 million cells. A number of the grid elements is limited, since correct operation of FlowVision requires a certain amount of computational power per each 1.5 million cells. A profile of the velocity near the wall was determined by a model of equilibrium wall functions WFFV (Wall functions FlowVision) [19].

The monitoring points shown in Fig. 3, *a* were used to control and record values of the temperature and the velocity components at each time step. In addition to the main monitoring points corresponding to the locations of the thermocouples in the experimental model, intermediate points were added for detail resolution of the fields of the thermal and hydrodynamic characteristics. The length of the calculated implementations was ≈ 150 s.

It is assumed in the study [20] that correct application of the LES-approach requires to reproduce at least 80 % of kinetic energy of turbulence. Hence, a cell (filter) size shall resolve structures that are related to a descending inertial interval of an energy range. The average cell size in the mixing zone was selected based on a Taylor microscale that characterizes sizes of the eddy structures, in which turbulent energy is largely dissipated.

A preliminary stationary calculation was done using a $k-\omega$ SST-model of turbulence [21] to obtain the fields of kinetic energy of turbulence k, its dissipation rate ε and kinematic viscosity ν, according to which integral l-, Kolmogorov η- and Taylor λ-scales are determined [21]:

$$l = \sqrt{\frac{3}{2}}\frac{k^{3/2}}{\varepsilon} = \sqrt{\frac{3}{2}}\frac{(3.5\cdot 10^{-4})^{3/2}}{0.019} \approx 0.42\,\text{mm}, \quad (15)$$

$$\eta = \sqrt[4]{\frac{\nu^3}{\varepsilon}} = \sqrt[4]{\frac{(4.3\cdot 10^{-7})^3}{0.019}} \approx 0.045\,\text{mm}, \quad (16)$$

$$\Delta = \lambda = \left(\frac{2}{3}\right)^{1/6}\sqrt{10}\cdot\eta^{2/3}\cdot l^{2/3}$$

$$= \left(\frac{2}{3}\right)^{1/6}\sqrt{10}\cdot(0.045)^{2/3}\cdot(0.42)^{1/3} \approx 0.28\,\text{mm}. \quad (17)$$

The selected element size makes it possible to resolve an energy-significant fluctuation range that characterizes specifics of the studied process and prevails when estimating the averaged characteristics.

In order to take into account the dependence of density, thermal conductivity, heat capacity and dynamic viscosity of the medium on the temperature, polynomial dependences at a working pressure are obtained in Ansys Fluent. The FlowVision software uses a substance database, where a set of the thermal-physical properties is represented as dependences on the temperature at the constant pressure.

Initial conditions for the nonstationary calculation using the WALE model were obtained as a result of solving a stationarily-formulated problem on the described grid model using the $k-\omega$ SST-model of turbulence. For boundary conditions for inlet cross sections of the „hot“ and „cold“ flows when solving the stationarily-formulated problem, we used stabilized velocity profiles, profiles of kinetic energy of turbulence k and its specific dissipation rate ω, which are obtained using a periodic boundary condition at specified values of the mass flow rate and the temperature (Table 1). During the nonstationary calculation, the stabilized velocity profiles and the constant temperature values were specified at inlet boundaries. A low degree of turbulence of the „hot“ flow in a feed channel as compared to the area downstream of the separation diffusor made it possible to avoid generation of synthetic turbulent fluctuations at the inlet.

Table 1. Parameters of the simulated regimes

No	Re_h	Re_c	G_h, kg/h	G_c, kg/h	T_h, °C	T_c, °C
1	69 000	1570	2460	34	72	22
2		3050		66		
3		790		17		

In the calculations using the Sm model, the inlet portion of the „hot“ flow was increased by 20 diameters, so was that of the „cold“ flow by 10 diameters, in order to form the stabilized velocity profiles upstream of the diffusor and a zone of injection of the „cold“ flow. The boundary conditions for the inlet cross sections of the model — the mass flow rate and the temperature (Table 1).

The solution of the nonstationarily-formulated problem is characterized by selection of a correct time step Δt, which was determined according to a criterion of stability of the numerical solution of the Courant-Friedrichs-Lewy differential equations (CFL) [22] to be 0.002 s.

It was simulated in Ansys Fluent using a confined pressure-based algorithm. At the same time, the equations of momentum and continuity are simultaneously solved, improving convergence of a solution. A system of linear algebraic equations (SLAE) was solved using an algebraic multi-grid method (AMG) with application of an F-cycle for stabilization of convergence [15]. Settings of the solution of the system of the differential equations are given in Table 2.

The Navier-Stokes equations are numerically solved in the FlowVision software by realizing an implicit method of splitting by physical variables [23]. The SLAE was solved using an AST adaptive technology which is a combination of aggregative (A) and selective (S) AMG methods as well as the TParFBSS solver of the GMRES type (T) [24,25]. In case of no convergence by a specified value of maximum discrepancy when using the A method, the AST solver is switched to the S method. And then, if necessary, it is transited to the most stable T method. The basic settings of the parameters of the numerical method are given in Table 3.

Table 2. Settings of the computational method in Ansys Fluent

Parameter	Solution diagram type
Discretization of a convective summand of the momentum equation	Method of bounded central differencing
Discretization of the convective summand of the energy equation	Counter-flow scheme of the second order of accuracy
Discretization of the diffusion summands of the transfer equations	Central-difference scheme of the second order of accuracy
Pressure interpolation	Scheme of the second order of accuracy
Calculation of gradients	Method of least squares in a cell (Linear approximation of the parameter in the cell)
Discretization of the time summand	Bounded second order of accuracy for implicit schemes
Number of internal iterations of the solver	10

Table 3. Settings of the computational method in FlowVision

Parameter	Solution diagram type
Discretization of the convective summands of the transfer equations	Scheme of the second order of accuracy
Discretization of the diffusion summands and calculation of the gradients of the transfer equations	Hybrid scheme with the transition from the second to the first order of accuracy
Discretization of the time summand	Implicit scheme of the first order of accuracy
Number of internal iterations of the solver	10

3. Analysis of results

The experimental simulation made it possible to distinguish three representative combinations of the regime parameters for numerical analysis (Table 1). The highest interest for validation of the computational model belongs to the regime No. 1 that is characterized by pronounced dynamism due to significant spatiotemporal fluctuations of the eddy area in the mixing zone. The modes Nos. 2 and 3 were selected for estimating sensitivity of the computational model to variation of the boundary conditions. A variable parameter was a flowrate of the „cold“ flow. Influence of variation of the boundary conditions was estimated by comparing computational-experimental distributions of the averaged characteristics.

Based on results of the LES-simulation, resolution of the computational model was analyzed based on refining the integral (15), Kolmogorov (17) and Taylor (16) spatial scales. The rate of dissipation of turbulent energy ε (18) in the mixing zone was calculated by means of the time-averaged velocity gradients that form the strain rate tensor [26]:

$$\varepsilon = 2\nu\langle|\overline{S}|^2\rangle \approx 0.025\,\mathrm{m}^2/s^3. \qquad (18)$$

The numerical values of the spatial scales were $l_{\mathrm{LES}} = 71.6$, $\eta_{\mathrm{LES}} = 0.042\,\mathrm{mm}$, $\lambda_{\mathrm{LES}} = 1.49\,\mathrm{mm}$. Comparison of the value of the Taylor microscale with a typical size of the grid element $\Delta/\lambda_{\mathrm{LES}} \approx 0.19$ confirms that spatial resolution of the eddy structures is correct.

Influence of the small-scale eddies on the resolved structures is related to the Kolmogorov time scale (19):

$$\tau_{\eta_{\mathrm{LES}}} = \left(\frac{\nu}{\varepsilon}\right)^{1/2} \approx 4.1 \cdot 10^{-3}\,\mathrm{s}. \qquad (19)$$

A ratio of the time step to the Kolmogorov time scale $\Delta t/\tau_{\eta_{\mathrm{LES}}} \approx 0.48$ meets requirements of the LES-approach and provides necessary conditions for quality operation of the subgrid model.

A dimensionless epure of an axial component of the velocity downstream of the diffusor (Fig. 4) makes it possible to estimate a length of the eddy area being formed, whose boundary is near the zone of injection. Under these conditions, a „cold“ laminar jet most effectively locally affects the wall of the main pipe, since the high degree of the turbulent fluctuations of the flow upstream of the mixing zone does not make it possible to form stable hydrodynamic and temperature boundary layers that affect fluctuations of the temperature field in a damper manner. Due to counter motion of the coolant flows with the equal values of the axial (V_Z) components of the velocity, a quasi-steady-state eddy area is formed under the peripheral tube cut. The computational-experimental distributions of the temperature

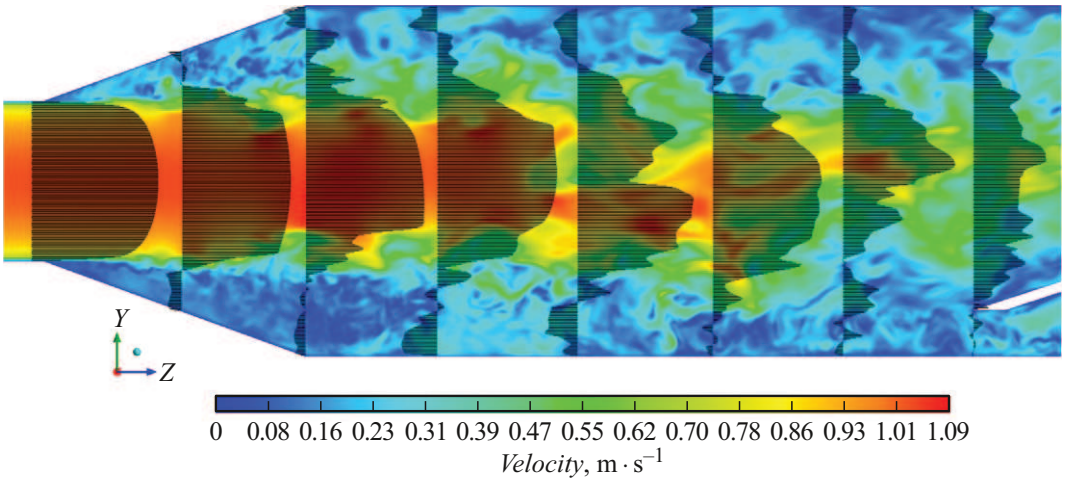

Figure 4. Typical velocity field (the WALE model) at the moment of time $t = 11.5$ s for the regime No. 1.

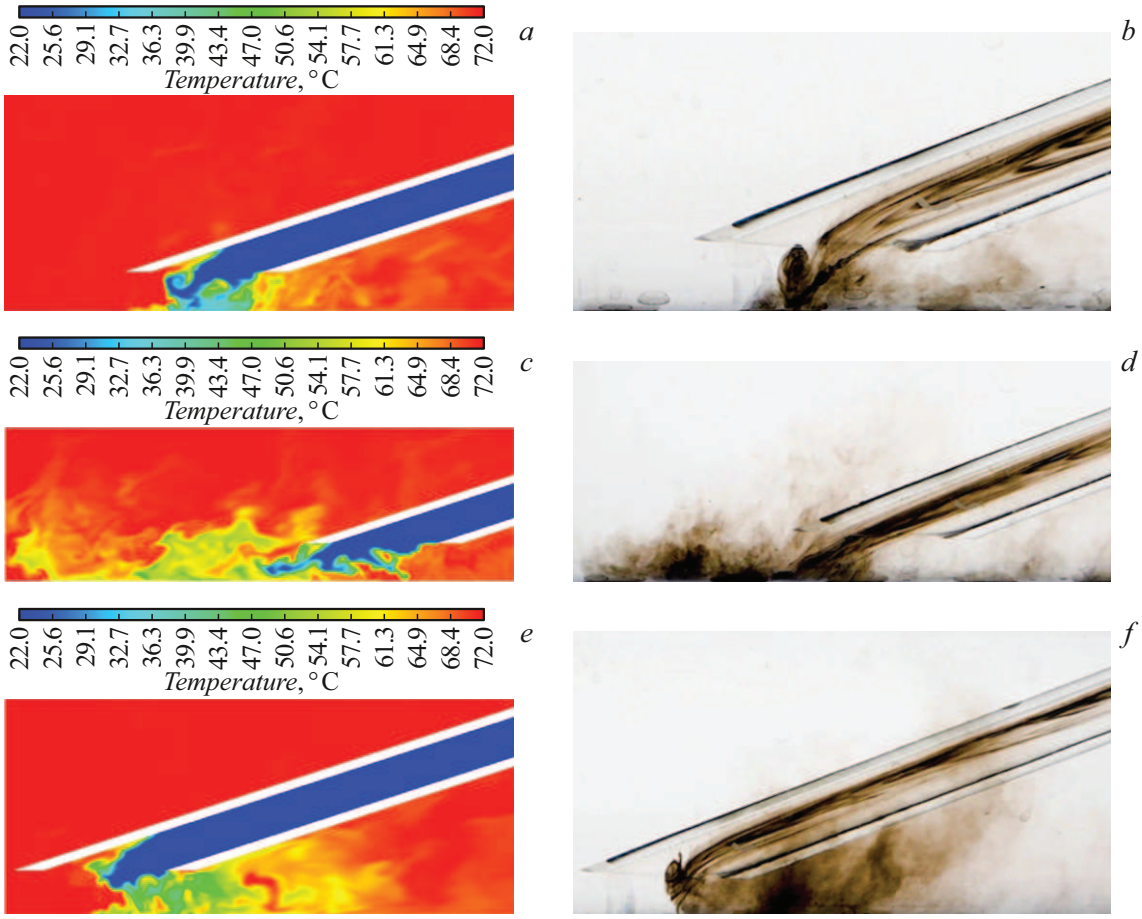

Figure 5. Instantaneous computational-experimental distributions of the temperature (the WALE model) and the tracer for the regime No. 1 when forming the quasi-steady-state eddy area (a, b), ejection of the „cold“ flow towards the diffusor (c, d) and „separation“ of the „cold“ flow towards an exit of the experimental model (e,f).

(the WALE model) and the tracer (Fig. 5, a, b) confirm this specific feature.

Frame-by-frame analysis of fragments of video records indicates a fluctuation of the eddy area, which is caused by irregular ejection of the „cold“ flow towards the diffusor (Fig. 5, c, d). Each ejection is characterized by sharp reduction of the temperature around the thermocouples Nos. 1 and 2 [9]. At the same time, there is traced

„separation“ of the „cold“ flow towards the exit of the experimental model (Fig. 5, *e*,*f*). The described specific features of eddy motion in the flow mixing area are attributed by the authors to alternate separation of the flow from opposite sides of the diffusor. The geometry of the diffusor and a combination of the regime parameters of the „hot“ flow provide significant oscillations of a size and a location of the separation zone as well as intensity of separation in time, thereby causing fluctuations of the eddy area in the mixing zone [27].

The computational-experimental profiles of the averaged temperature and intensity of fluctuations (a mean-square deviation) of the flow temperature was compared by means of a dimensionless temperature T^* [28]:

$$T^* = \frac{T - T_x}{T_r - T_x} \tag{20}$$

where T is an instantaneous value of the medium temperature.

The time-averaged value of the dimensionless temperature was determined:

$$\overline{T^*} = \frac{1}{N}\sum_{i=1}^{N} T^*, \tag{21}$$

where N is a number of counts.

Intensity of fluctuations of the dimensionless temperature was calculated as follows:

$$T^*_{\mathrm{RMS}} = \sqrt{\frac{1}{N}\sum_{i=1}^{N}(T^* - \overline{T^*})^2}. \tag{22}$$

A quantitative estimate of the deviation of the computational-experimental distributions for M points was calculated by the formula:

$$\sigma(x) = \sqrt{\sum_{i=1}^{M}\frac{(x_i^{calc} - x_i^{exp})^2}{M}}. \tag{23}$$

Despite better compliance of the profiles of $\overline{T^*}$ (Fig. 6, *a*) and T^*_{RMS} (Fig. 6, *b*) for the experiment and the calculation using the Sm model ($\sigma_{\mathrm{Sm}} < \sigma_{\mathrm{WALE}}$), local specific features of the studied process are represented more accurately by the WALE model. Around the points T_4–T_6, there is an area of maximum temperature gradients being formed, which originates due to active interaction of the counter flows. The WALE model quite accurately reproduces a minimum of the averaged temperature, which is observed in Fig. 6, *a*. The maximum value of intensity of fluctuations for WALE is located near the point T_4 that corresponds to the boundary of the eddy area downstream of the diffusor (Fig. 4) and the zone of injection of the „cold“ flow. Intense transfer of momentum by the large-scale structure in the said area initiates turbulent mixing of the „cold“ jet with the „hot“ flow, thereby explaining the observed maximum of intensity of thermal fluctuations. It should be noted here that a general nature of the experimental distributions is qualitatively described by both the computational models.

The regime No. 2 (Fig. 6, *c*, *d*) is characterized by a high value of the flowrate of the „cold“ flow and, as a result, an increased frequency of its ejection towards the diffusor. It is noticeable when analyzing the fragments of the computational-experimental implementations that (Fig. 7) Sm much more often reproduce ejection of the „cold“ flow (Fig. 7, *e*) as compared to the experiment (Fig. 7, *a*) and WALE (Fig. 7, *c*). Moreover, implementation of the temperature in the point T_3 demonstrates a prevailing stream of the „cold“ flow (Fig. 7, *f*). A fragment of the experimental implementation (Fig. 7, *b*) is characterized by a slow increase of the temperature after impact by the „cold“ medium, since it is difficult to record fast processes by means of the thermocouples due to their higher inertness as compared to the calculations. The above-said results in reduced values of the average temperature in the considered area (Fig. 6, *c*). Despite a significant divergence of the profile, the WALE model instantaneously restores the value of the temperature after impact by the „cold“ flow (Fig. 7, *d*).

The computational-experimental distributions of T_{RMS^*} (Fig. 6, *d*) appear similarly. Both the subgrid models are characterized by precise localization of the area with the highest value of intensity of fluctuations near the point T_4.

The profile $\overline{T^*}$ (Fig. 6, *e*) for the regime No. 3 (Table 1) obtained using the WALE model in a higher degree ($\sigma_{\mathrm{Sm}} > \sigma_{\mathrm{WALE}}$) corresponds to the experimental profile. Despite a significant divergence of the profiles of T^*_{RMS} (Fig. 6, *f*), which is related to inertia properties of the thermocouples, the general nature of the distribution is still the same. Reduction of the flowrate of the „cold“ flow increases a frequency of its separation along the direction of motion of the „hot“ flow. This method contributes to reduction of the maximum means-square amplitude of fluctuations int he mixing zone and shifting the maximum of the profile T^*_{RMS} to the right in relation to the regime No. 1. The computational models take into account the described specifics of the regime No. 3.

A significant difference of the approaches to closing of τ_{ij} makes it possible to assume that the WALE model more accurately reproduces the flow structure in the mixing zone. According to (14), the dependence of $|\overline{S}|$ only on the symmetric part $\overline{S}_{ij}$ of the velocity gradient tensor can result in formation of excessive turbulent diffusion. The Sm standard model interprets any velocity gradients as a dissipation source. Be generating artificial subgrid viscosity in the area of the laminar „cold“ flow [17], Sm seems to contribute to distortion of dynamics of turbulence in the mixing zone. An artificial growth of turbulent diffusion μ_t/Pr_t in the energy equation (4) results in excessively intense mixing. On the contrary, when calculating μ_t the WALE model uses an invariant $S^d_{ij}S^d_{ij}$ that takes into account join influence of the symmetric $\overline{S}_{ij}$ and antisymmetric $\overline{\Omega}_{ij}$

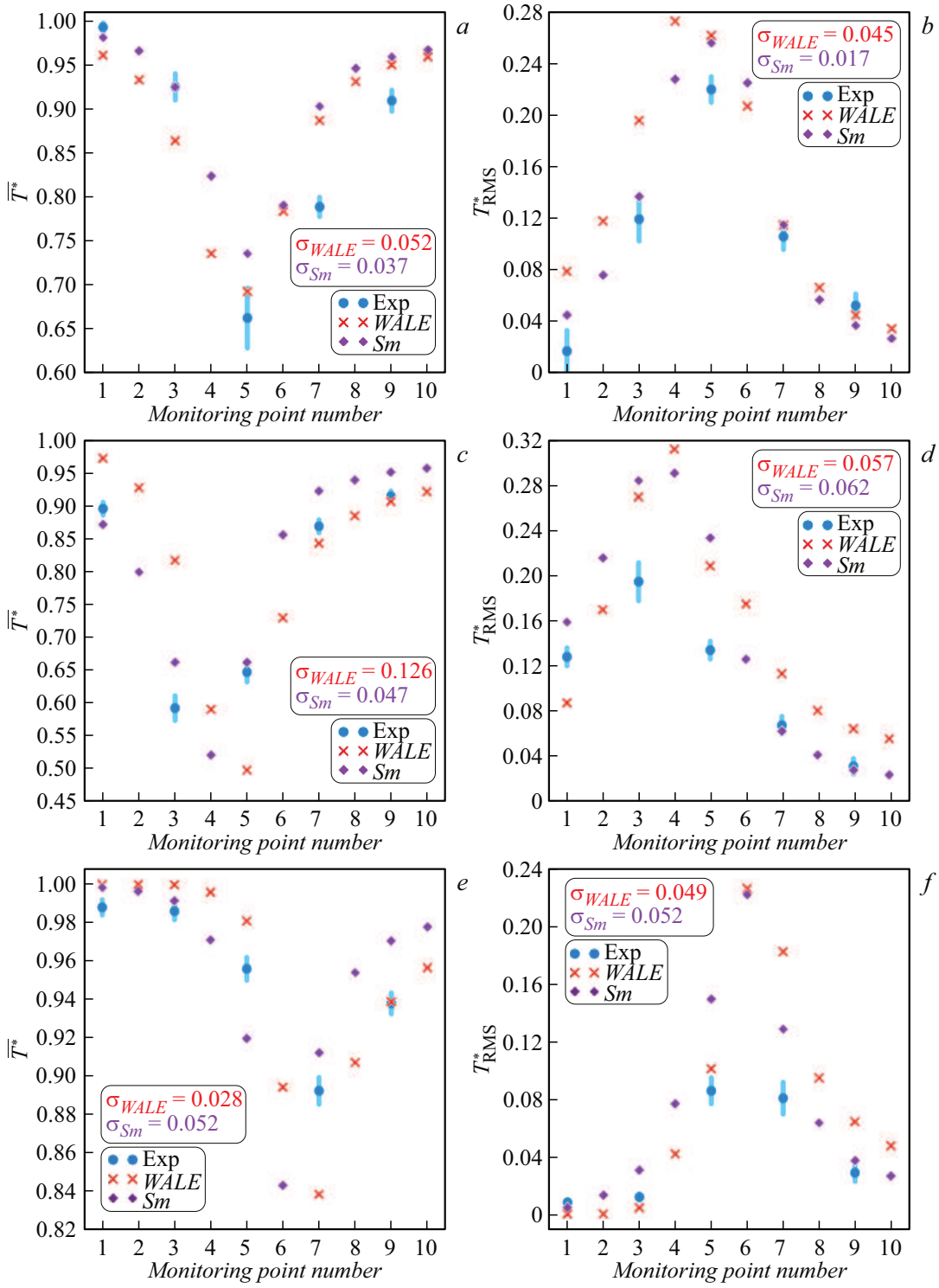

Figure 6. Averaged profiles of the dimensionless temperature and temperature fluctuation intensity for the regime No. 1 (a, b), the regime No. 2 (c, d) and the regime No. 3 (e, f).

parts of the velocity gradient tensor. It makes it possible to generate μ_t in the zones of developed turbulence, which are characterized by simultaneous deformation and rotation, effectively dissipating energy at the subgrid level. Taking into account the discussed specifics of the models, it can be presumed that while keeping energy of the large eddies WALE more correctly describes the processes of mixing and heat transfer without excessive damping of fluctuations. Along with the subgrid closing models, one should also note other important methodological factors that affected the noticeable divergence of the calculation results. The FlowVision software used the automatically-generated grid

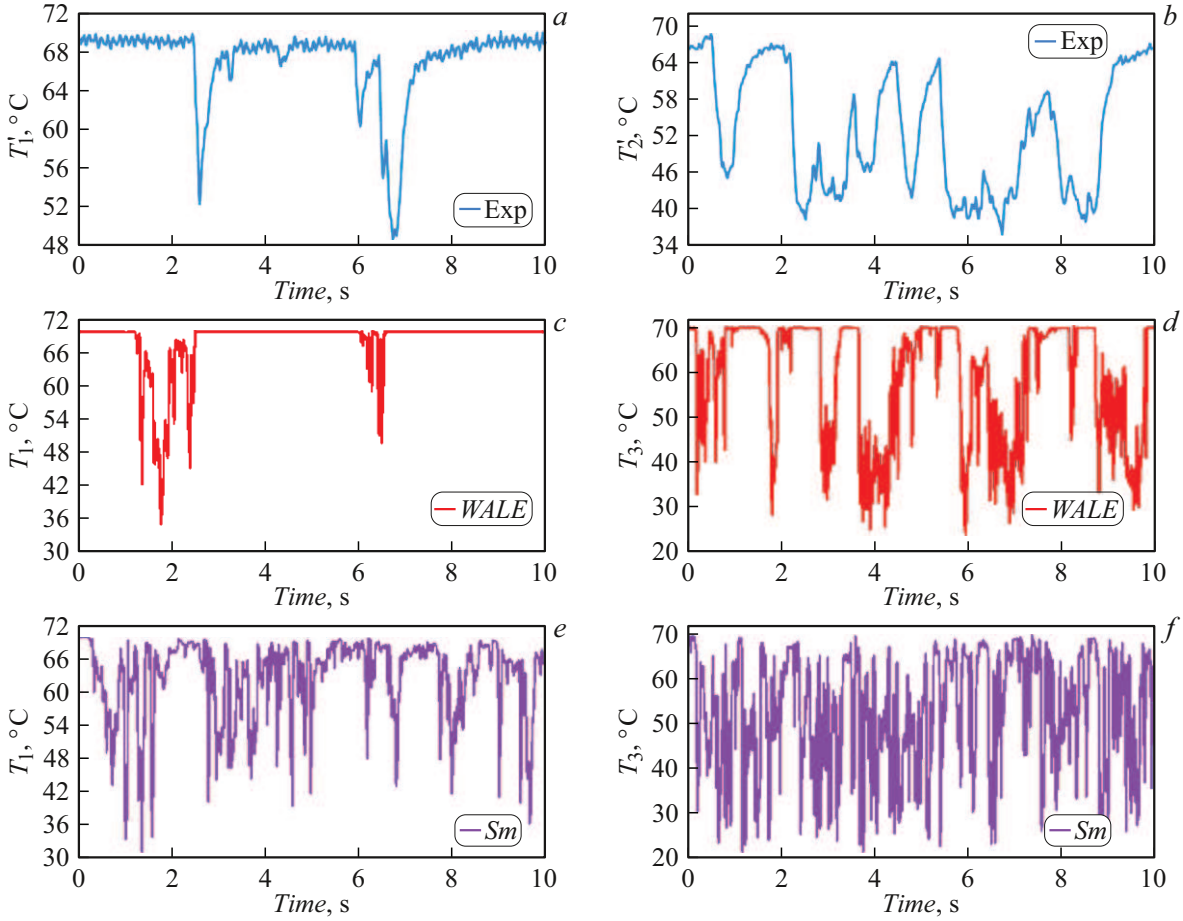

Figure 7. Fragments of implementations of the temperature for the regime No. 2: recorded by the thermocouplesT_1 (a) and T_2 (b); obtained using the models WALE (c,d) and Sm (e,f) in the points T_1 and T_3.

model with coarser spatial discretization of the mixing area (Fig. 3, b), thereby undoubtedly limiting resolution of the computational model and resulting in smoothing of sharp parameter gradients. Presently, functional capabilities of FlowVision in terms of discretization of the summands of the transfer equations are limited by schemes shown in Table 3. It is obvious that using the first order of accuracy for discretization of the time summand amplified influence of scheme diffusion on the range of resolvable scales, damping turbulent fluctuations at the same time. No turbulent content at the inlet boundary of the „hot" flow in Fluent did not affect the structure of the flow downstream of the diffusor. A point of „adhesion" of the „hot" flow to the main pipe wall (Fig. 4) is located around the point T_4, where intensity of temperature fluctuations has the highest value [6]. The set of the said specific features of the computational model in FlowVision causes its higher dissipativity, which could partially compensate inertness of the thermocouples. It is difficult to estimate a contribution by each aspect herein, thereby requiring additional studies.

Calculation of spectral characteristics of temperature fluctuations is based on a technique discussed in [29]. The initial implementations were centered (24), the Fourier transform was done (25) and the power spectral density was calculated (26):

$$\langle T_j \rangle = T_j - \langle T \rangle = T_j - \frac{1}{N}\sum_{j=1}^{N} T_j, \quad j = 1, 2, \ldots N, \quad (24)$$

$$F(\nu)_k = \frac{1}{\sqrt{N}}\sum_{j=1}^{N}\langle T_j \rangle \cdot e^{-2\pi i \cdot \frac{j}{N}\cdot k},$$

$$\nu_k = \frac{k \cdot f}{N} = \frac{k}{N \cdot \Delta t}, \quad k = 1, 2, \ldots N/2, \quad (25)$$

$$\mathrm{PSD}_k = 2|F(\nu)_k|^2, \quad r\mathrm{PSD}_k = \mathrm{PSD}_k / \max(\mathrm{PSD}_k). \quad (26)$$

The main energy of computational-experimental spectra is concentrated within a frequency range $f = 0{-}1$ Hz and corresponds to the area of energy-carrying eddies (Fig. 8). In the studies [7,8], the authors noted presence of the pronounced energy maximum around the frequency $f = 0.4$ Hz. A frequency of fluctuations at the said frequency is not high, but presence of this local maximum indicates a high degree of accuracy of simulating the flow part of the experimental branch of the high-temperature bench (Fig. 8). Despite a more complicated structure,

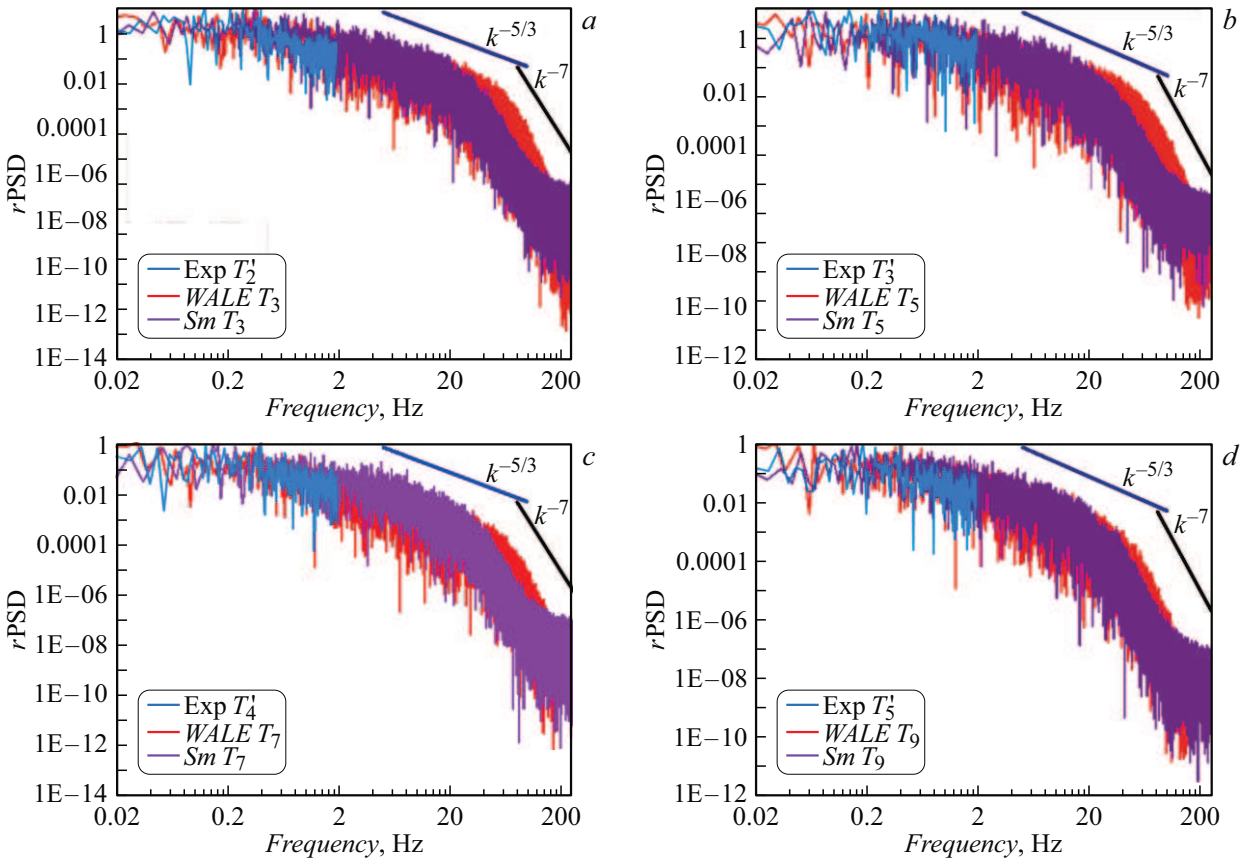

Figure 8. Power spectral density of fluctuations of the temperature for the regime No. 1: *a* — in the point T_3 (the thermocouple T_2); *b* — in the point T_5 (the thermocouple T_3); *c* — in the point T_7 (the thermocouple T_4); *d* — in the point T_9 (the thermocouple T_5).

the spectra of the computational implementations also demonstrate presence of the same maximum.

We observe the inertial interval of transfer of energy of temperature fluctuations, which obeys the Kolmogorov law „−5/3“ and is also illustrated in Fig. 8. A range of cascade transfer of fluctuation energy, which is obtained in Ansys Fluent, is within the frequency range $f = 1-50$ Hz, and it is within $f = 1-20$ Hz for FlowVision.

An early cut-off of the inertial interval in FlowVision is related to increased dissipativity of the computational model. Uncertainty of selecting the value of an empirical constant of the Sm model, which generally requires calibration in a dependence on a numerical method used [13], could additionally affect a spectrum shape. A sharp decline of the spectrum with a typical slope of „−7“ is a result of numerical dissipation. For WALE this area is localized within the range $f = 50-150$ Hz, while for Sm $- f = 20 - 110$ Hz.

The computational spectra of temperature fluctuation power are identical to a one-dimensional energy spectrum of developed isotropic turbulence as per Heisenberg [30,31], in which the distribution of turbulent fluctuation energy is described by the equation:

$$E(k) = \frac{4\gamma^2}{\varepsilon}\tilde{k}^{-\frac{5}{3}}\left(\frac{3\gamma^2}{\varepsilon} + C\cdot\tilde{k}\right)^{-\frac{4}{3}}, \qquad (27)$$

where $\tilde{k}$ is a wave number; ε is the energy dissipation rate; γ and C — constants.

In order to obtain comprehensive information about specific features of hydrodynamics of the studied process, profiles of kinetic energy of turbulence (28) were analyzed. The numerical value of this magnitude makes it possible to estimate intensity of velocity fluctuations in the flow, identifying specifics of formation of the large-scale eddy structures and their spatial evolution.

$$k = \frac{1}{2}\left(\overline{V'^2_X} + \overline{V'^2_Y} + \overline{V'^2_Z}\right), \qquad (28)$$

where $\overline{V'^2_X}, \overline{V'^2_Y}, \overline{V'^2_Z}$ are mean-square components of the fluctuation velocity.

A high level of turbulent fluctuations in the points T_1-T_3 (Fig. 9), which is observed for all the modes, is due to the separation stream downstream of the diffusor. Collapse of a coherent structure of the constrained jet due to its interaction with the decelerated surrounding flow results in formation of macroeddies of various scales (Fig. 10). Rotation of the large-scale eddy structures is associated with their tensioning that increases the vorticity flow (Fig. 10, the area marked by the black color) [32], thereby keeping a significant level of fluctuations. An intense decline of energy around the point T_5 for the modes No. 1 (Fig. 9, *a*)

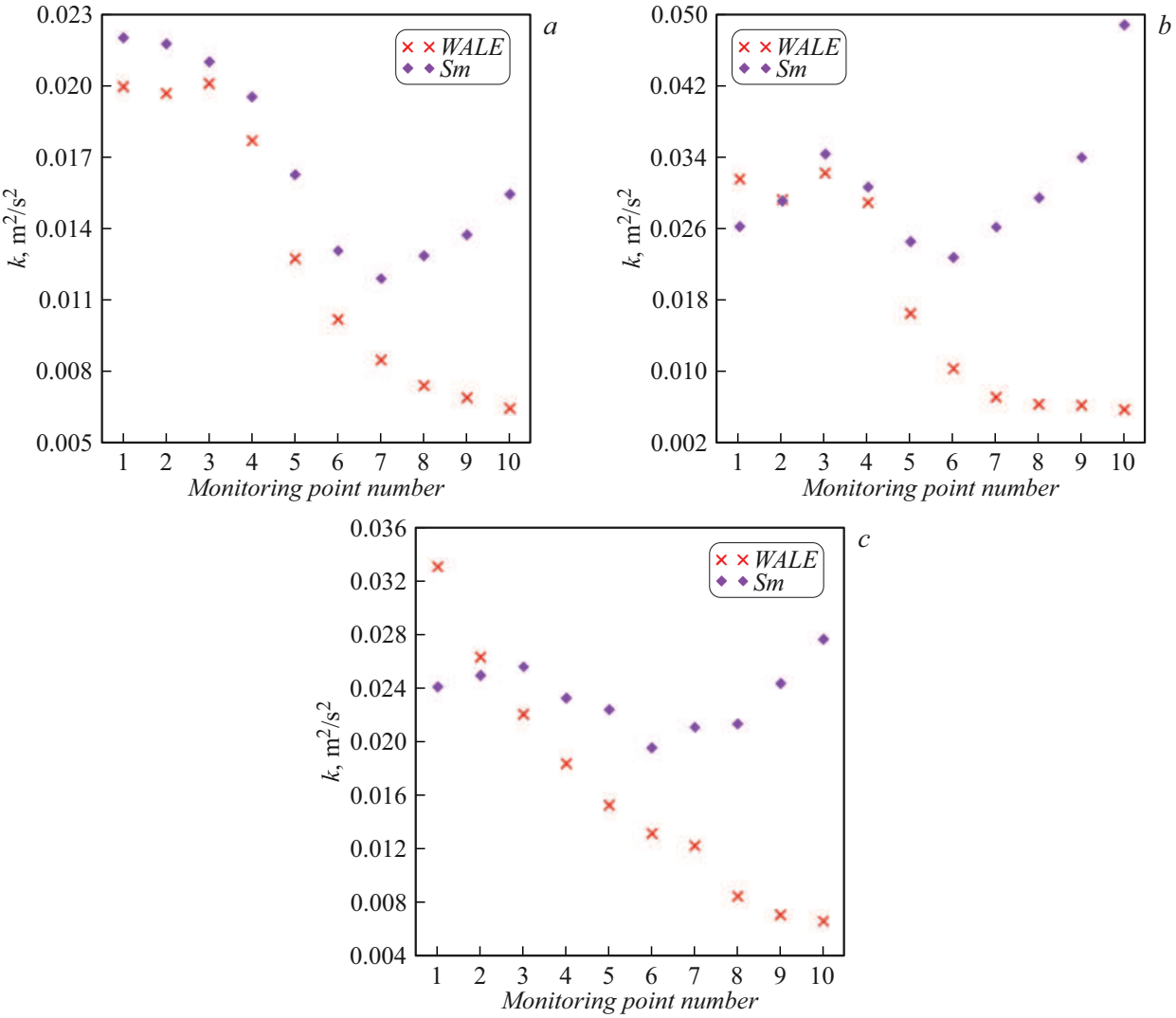

Figure 9. Calculated profiles of kinetic energy of turbulence for the regime No. 1 (*a*), the regime No. 2 (*b*) and the regime No. 3 (*c*).

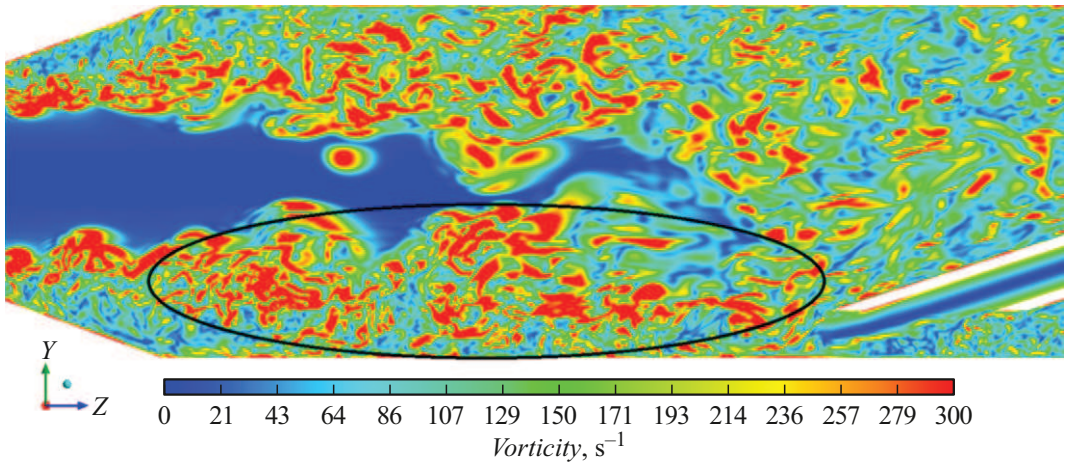

Figure 10. Typical vorticity field (the WALE model) at the moment of time $t = 12.7$ s for the regime No. 1.

and No. 2 (Fig. 9, *b*) is caused by collision of counter coolant flows. Under the peripheral tube cut, there is a small-scale eddy area (Fig. 5, *a*, *b*) being formed, which is oriented perpendicular to the direction of motion of the „hot" flow. Sharp reduction of the strain rate in the said area, which is related to a laminar structure of the „cold" flow, damps intensity of longitudinal fluctuations. Starting from the point No. 6, the WALE model gradually forms the boundary layer that facilitates smooth reduction of the level of turbulent fluctuations and smoothing of the velocity profile. The regime No. 3 (Fig. 9, *c*) in the entire considered area is characterized by a uniform decline of energy due to a low value of the flowrate of the „cold" flow, which does not significantly affect scattering of eddy energy.

An increase of energy of turbulent fluctuations when calculating in FlowVision starting from the point No. 7 for the regime with $\mathrm{Re}_c = 1570$ and the point No. 6 for the modes with $\mathrm{Re}_c = 790$ and 3050 reflects complex influence of methodological specific features: a fixed value of the constant of the Sm model, which is not calibrated for the FlowVision schemes; total dissipativity of the computational model. In turn, this could result in local redistribution of energy in the zone downstream of the peripheral tube.

Conclusion

The present study included complex simulation of the mixing process in the originally-designed Y-junction. The experimentally-found combinations of the regime parameters made it possible to validate the computational model and to estimate its capability of reliably describing hydrodynamics of the stream and its related temperature field when varying the boundary conditions. Dynamics of the turbulent structures was computationally simulated by an eddy-resolving LES-approach using the subgrid models WALE and Sm. The eddy structures were spatiotemporally resolved with a time step of 0.002 s.

The calculated profiles of the dimensionless characteristics for the regime No. 1 qualitatively agree with the experimental distributions. The best quantitative compliance with the experimental profiles was demonstrated by the Sn model. Due to higher dissipativity of the FlowVision computational model, it is assumed that excessive diffusion of the model and inertness of the thermocouples are mutually compensated, which can result in loss of important information during computational simulation of such processes. Sensitivity of the computational model to variation of the boundary conditions has been analyzed to demonstrate that the numerical approach selected together with the WALE model is successively adapted to variation of input parameters of the problem at fixed settings of a computational algorithm. The fragments of computational and experimental video records made it possible to find hydrodynamic specific features of the eddy area that fluctuates in the mixing zone. The calculated distributions of fluctuation energy across the frequencies fully correspond to the experimentally-obtained spectrum of temperature fluctuations. Presence of the pronounced inertial interval indicates the developed process of cascade energy transfer. For FlowVision, an early cut-off of the inertial interval is observed and it is caused by increased dissipativity of the computational model. The profiles of kinetic energy of turbulence have been analyzed to identify the mechanism of formation of the large-scale eddy structures downstream of the diffusor and their influence on specifics of the process of mixing of the counter coolant flows.

The numerical approach based on using the WALE model and the unit topology quite precisely reproduced specific features of the mixing process and will be used for validating the computational technique of estimation of fatigue durability of structural materials of NPP equipment under random thermocyclic loads. The calculated profiles of turbulent energy can be used for calibrating the constants of empirical models of turbulence.

Conflict of interest

The authors declare that they have no conflict of interest.

References

[1] F.M. Mitenkov, V.B. Kaidalov, Yu.G. Korotkih, V.A. Panov, S.N. Pichkov. *Metody obosnovaniya resursa yadernykh energeticheskih ustanovok* (Mashinostroenie, M., 2007) (in Russian).

[2] A.V. Sudakov, A.S. Trofimov. *Pul'satsii temperatur i dolgovechnost' elementov energooborudovaniya* (Energoatomizdat, LO, L., 1989) (in Russian).

[3] M.S. Chen, H.E. Hsieh, Y.M. Ferng, B.S. Pei. Nucl. Eng. Des., **276**, 107 (2014). DOI: 10.1016/j.nucengdes.2014.03.052

[4] G.Y. Chuang, Y.M. Ferng. Appl. Therm. Eng., **113**, 1585 (2017). DOI: 10.1016/j.applthermaleng.2016.10.157

[5] P. Karthick Selvam, R. Kulenovic, E. Laurien, J. Kickhofel, H.-M. Prasser. Nucl. Eng. Des., **322**, 32 (2017). DOI: 10.1016/j.nucengdes.2017.06.041

[6] S.M. Dmitrie, R.R. Ryazapov, A.V. Mamaev, A.E. Sobornov, A.V. Kotin, M.A. Legchanov, A.V. L'vov. Pribory i metody izmerenii, **10** (1), 53 (2019) (in Russian). DOI: 10.21122/2220-9506-2019-10-1-53-60

[7] S.M. Dmitriev, A.V. Mamaev, R.R. Ryazapov, A.Ye. Sobornov, A.V. Kotin, D.Ye. Bescherov, M.A. Bolshukhin. NUCET, **5** (3), 225 (2019). DOI: 10.3897/nucet.5.39319

[8] R.R. Ryazapov, A.E. Sobornov, S.M. Dmitriev, N.V. Matsin, A.V. Kotin. Izvestiya vuzov. Yadernaya energetika, **1**, 57 (2023) (in Russian). DOI: 10.26583/npe.2023.1.05

[9] R.R. Ryazapov, A.V. Mamaev, A.E. Sobornov, A.M. Kuskov, I.A. Kudahskin. VANT. Seriya: Yderno-reaktornye konstanty, **2**, 203 (2023) (in Russian).

[10] P. Kakka, K. Anupindi. Int. J. Heat Mass Transfer, **153**, 119593 (2020). https://doi.org/10.1016/j.ijheatmasstransfer.2020.119593

[11] M. Bergagio, W. Fan, R. Thiele, H. Anglart. Nucl. Eng. Des., **356**, 110361 (2020). DOI: 10.1016/j.nucengdes.2019.110361
[12] C. Evrim, X. Chu, E. Laurien. Int. J. Heat Mass Transfer, **158** (6), 120019 (2020). DOI: 10.1016/j.ijheatmasstransfer.2020.120019
[13] A.V. Garbaruk, M.Kh. Strelets, M.L. Shur. *Modelirovanie trubulentnosti v raschetakh slozhnykh techenii* (Izd-vo Politekhn. un-ta, SPb., 2012) (in Russian).
[14] F. Nicoud, F. Ducros. Flow, Turbulence Combustion, **62** (3), 183 (1999). DOI: 10.1023/A:1009995426001
[15] ANSYS, Inc. *ANSYS Fluent Theory Guide v19.0* (ANSYS Inc., Canonsburg, 2018)
[16] I.A. Belov, S.A. Isaev. *Modelirovanie turbulentnykh techenii* (BGTU, SPb., 2001) (in Russian).
[17] M. Kim, J. Lim, S. Kim, S. Jee, D. Park. Comput. Methods Appl. Mech. Eng., **371** (1), 113287 (2020). DOI: 10.1016/j.cma.2020.113287
[18] A.A. Aksenov, A.A. Dyadkin, V.I. Pokhilko. *Proc. of 1998 ASME Pressure Vessels and Piping Division Conference* (San Diego, USA, 1998), v. 377−1.
[19] S.V. Zhlutkov, A.A. Aksenov. Komp'yuternye issledovaniya i modelirovaniye, **7** (6), 1221 (2015) (in Russian). DOI: 10.20537/2076-7633-2015-7-6-1221-1239
[20] S.B. Pope. *Turbulent Flows* (CUP, Cambridge, 2000)
[21] A.Yu. Snegirev. *Vysokoproizvoditel'nye vychisleniya v tekhnicheskoi fizike. Chislennoe modelirovanie turbulentnykh techenii* (Izd-vo Politekhn. un-ta, SPb., 2009) (in Russian).
[22] R.J. LeVeque. *Finite Volume Methods for Hyperbolic Problems* (CUP, Cambridge, 2002)
[23] A.A. Aksenov, S.V. Zhlutkov, V.I. Pokhilko, K.E. Sorokin. Komp'yuternye issledovaniya modelirovanie, **15** (4), 1009 (2023) (in Russian). DOI: 10.20537/2076-7633-2023-15-4-1009-1023
[24] S.A. Kharchenko. Vychislitel'nye metody i programmirovanie, **11** (4), 373 (2010) (in Russian).
[25] V.L. Yakushev, V.N. Simbirkin, A.V. Filimonov, P.A. Novikov, I.N. Kon'shin, G.B. Sushko, S.A. Kharchenko. Vestnik Nizhegorodskogo un-ta im. N.I. Lobachevskogo, (4−1), 238 (2012) (in Russian).
[26] P. Sagaut. *Large Eddy Simulation for Incompressible Flows* (Springer, Heidelberg, 2006)
[27] I.E. Idel'chik. *Spravochnik po gidravlicheskim soprotivleniyam*, pod red. M.O. Shteinberga (Mashinostroenie, M., 1992), s. 672 (in Russian).
[28] Z. Nan, X. Zhao, Y. Li, K. Zhang, N. Wang. Int. J. Heat Mass Transfer, **181**, 121834 (2021). DOI: 10.1016/j.ijheatmasstransfer.2021.121834
[29] P. Buchhave, C. Velte. Phys. Fluids, **29** (8), 085109 (2017). DOI: 10.1063/1.4999102
[30] S.V. Borisenok. Izvestiya RGPU im. A.I. Gertsena,, **5** (13), 104 (2005) (in Russian).
[31] E. Sirbubalo, Ph.D. Thesis. (Darmstadt, Technische Universität Darmstadt, 2012)
[32] K.N. Volkov, V.N. Emel'yanov. *Modelirovanie krupnykh vikhrei v raschetakh turbulentnykh techenii* (Fizmatlit, M., 2008) (in Russian).

Translated by M.Shevelev